Mitigation Method of Slot Harmonic Cogging Torque Considering Unevenly Magnetized Permanent Magnets in PMSM

Chaelim Jeong [1], Dongho Lee [2] and Jin Hur [3,*]

[1]   Department of Industrial Engineering, University of Padova, 35131 Padova, Italy; cofla827@gmail.com
[2]   Sungshin Precision Global (SPG) Co., Ltd., Incheon 21633, Korea; leedh38126@gmail.com
[3]   Department of Electrical Engineering, Incheon National University, Incheon 22012, Korea
*   Correspondence: jinhur@inu.ac.kr; Tel.: +82-10-4024-1728

check for
updates

Abstract: This paper presents a mitigation method of slot harmonic cogging torque considering unevenly magnetized magnets in a permanent magnet synchronous motor. In previous studies, it has been confirmed that non-uniformly magnetized permanent magnets cause an unexpected increase of cogging torque because of additional slot harmonic components. However, these studies did not offer a countermeasure against it. First, in this study, the relationship between the residual magnetic flux density of the permanent magnet and the cogging torque is derived from the basic form of the Maxwell stress tensor equation. Second, the principle of the slot harmonic cogging torque generation is explained qualitatively, and the mitigation method of the slot harmonic component is proposed. Finally, the proposed method is verified with the finite element analysis and experimental results.

Keywords: cogging torque; permanent magnet machine; torque ripple; uneven magnets

1. Introduction

The cogging torque is one of the most representative components of torque ripple in the permanent magnet synchronous motor (PMSM). Therefore, studies on the reduction method for the cogging torque have been actively carried out to minimize the torque ripple [1–11]. Those studies on cogging torques have been mainly focused on reducing the cogging effect by modulating the combination of the pole and slot number, the pole arc, the shape of the core, the skew angle, the notching, etc. In general, the results of such studies are based on a simple theoretical analysis, so it is assumed that the magnetic components of the motor are ideal. However, since there are many possible manufacturing errors such as eccentricity, machining error, and unevenly magnetized magnets, motors always contain non-ideal components. As a result of those errors, the measured cogging torque of the actual motor may be very different from what is expected in the simulation [12]. This phenomenon can be a critical issue to those applications that need precision control of the motor and are sensitive to noise and vibration.

For this reason, several studies that take manufacturing errors into consideration have emerged [13–19]. In [13–16], analytical solutions of cogging torque are studied by considering the magnet imperfections, rotor eccentricity, geometrical variation, and magnetizing fixture. In addition, [17] mathematically investigated the cogging torque caused by the simultaneous existence of eccentricities and the uneven magnetization. Those studies have focused on analysis methods of cogging torque by considering manufacturing errors, and they reported that those errors generate additional harmonic components. In [18], they show that the unevenly magnetized permanent magnet (PM) can have a negative impact on applying the cogging torque reduction method (teeth curvature modulation method), leading to additional slot harmonic cogging torque. In [19], it is confirmed that

the main contributors, which have the greatest effect on the cogging torque distortion, are the inner radius tolerance of the stator and the tolerance of PM remanence (unevenly magnetized magnets), among many other manufacturing errors. In addition to the aforementioned studies, there are a few studies that have analyzed motor performance in consideration of manufacturing errors, but those studies only handle the phenomena analysis caused by them, and there is a lack of research on the mitigation countermeasures.

Unlike most studies that have only analyzed the effects of manufacturing errors on cogging torque, this paper proposes a method to counteract the influence of unevenly magnetized magnets, which are one of the main contributors of cogging torque distortion [19]. Here, unevenly magnetized magnets mean that each magnet has different magnetic strength. This study is carried out in the following order. First, the relationship between the remanence of each PM and the cogging torque is derived from the basic form of the Maxwell stress tensor equation. Second, the principle of slot harmonic cogging torque generation is explained qualitatively. Based on this principle, a new mitigation method of slot harmonic cogging torque is proposed. This method involves a series of processes that select the position of the PMs, taking into account the remanence deviations of each PM. Finally, the proposed method is verified with a finite element analysis (FEA) and experimental results. Here, note that this study assumed that each magnet is pre-magnetized before the assembly. Therefore, the proposed method is more appropriate for small quantity customized production than mass production. Moreover, based on the principle of the slot harmonic component mitigation condition, it is possible to adjust that the manufacturing tolerance of the magnetization yoke, leading to the alleviation of the influence of the uneven magnetization.

2. Analysis of Cogging Torque in PMSM from a Macroscopic Perspective

Before examining the process of the slot harmonic cogging torque generation caused by the unevenness in magnetic strengths of each pole, we first analyzed the generation of cogging torque from a macroscopic perspective.

2.1. The Relation between the Electromagnetic Force and the Remanence of Magnet

The cogging torque refers to a torque caused by an electromagnetic force generated when the PM's magnetic flux passing through the air gap between a rotor and a stator is concentrated in a path that has a relatively small magnetic reluctance. Therefore, in order to analyze the magnitude of the cogging torque, it is necessary to understand the electromagnetic force. In many studies, according to Maxwell stress tensor theory, the electromagnetic force of the tangential component is defined as follows in a single rotor position [13,20–22]:

$$F_t = \frac{R}{\mu_0} \int_0^{2\pi} B_{rgap}(\phi_r) B_{tgap}(\phi_r) d\phi_r \tag{1}$$

where F_t is the tangential force density, μ_0 is the permeability of free space, R is the radius for which the Maxwell stress tensor is calculated, Φ_r is the space angle at single rotor position, and B_{rgap} and B_{tgap} represent radial and tangential components of magnetic flux density, respectively. Here, if the saturation phenomenon of the magnetic material is ignored, B_{rgap} and B_{tgap} are always proportional to the remanence of the PM (B_r), and the following relationship holds:

$$F_t \propto B_r^2 \tag{2}$$

2.2. The Cogging Torque Caused by Single Pole

The cogging torque according to the electromagnetic force described above can be defined as follows:

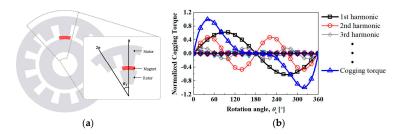$$T_{cog}(\theta, l) = R \int_0^{L_{stk}} F_t(\theta, l) dl \tag{3}$$

where θ is rotation angle of the rotor, L_{stk} is stack length, and l is axial length. Here, if the electromagnetic force is uniformly distributed in the stacking direction, the above equation can be simplified as the following equation:

$$T_{cog}(\theta) = RL_{stk}F_t(\theta) \tag{4}$$

To understand the period of cogging torque and the interaction of harmonic components, we first assumed an example model with one magnet (pole), as in Figure 1. Here, the pole-arc of the PM is 24° and the stator has 12 teeth. In this case, since the influences of eccentricity and shape error are deviated from the subject of this study, the cogging torque can be expressed in the following form of the Fourier series [23]:

$$T_{cog}(\theta) = RL_{stk}\sum_{k=1}^{\infty} F_{tk}\sin(kS\theta) = RL_{stk}\sum_{k=1}^{\infty} F_{tk}\sin(k\theta_s) \tag{5}$$

where θ_s is a slot periodic angle that is calculated by multiplying θ (mechanical angle) with the slot number, F_{tk} is Fourier coefficient (amplitude of force) of the 'k'th harmonic component, and S is the number of the slots.

Figure 1. (**a**) The geometry of the example model with one pole and twelve teeth; (**b**) cogging torque harmonic component due to one pole rotation (θ_s).

The cogging torque result of the example model of Figure 1a is shown in Figure 1b with the harmonic component. Here, the magnitude of each harmonic component is normalized to the peak value of the total cogging torque. Since the first harmonic component is the largest, the total cogging torque has the same period as the first harmonic component.

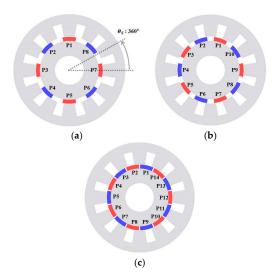### 2.3. The Cogging Torque Caused by Multi Poles

Now suppose that we add some magnets to the example model. Figure 2a–c have 8 poles, 10 poles, and 14 poles, respectively. Each added pole has the same remanence, pole-arc, and thickness. In this case, the cogging torque generated in each adjacent pole has a phase difference by a pole pitch. Further, due to the phase difference, the cogging torques generated by each pole interfere with each other. Using the property from Equation (5), the cogging torque caused by multi-poles can be expressed as follows using superposition technique [24,25].

$$\begin{aligned}
T_{cog}(\theta_s) &= T_{p1} + T_{p2} + T_{p3} + \cdots + T_{pP} \\
&= RL_{stk}\Bigg\{ \sum_{k=1}^{\infty} F_{t1_k}\sin(k\theta_s) + \sum_{k=1}^{\infty} F_{t2_k}\sin\left[k\left(\theta_s + (n_2 - 1)\frac{2\pi S}{P}\right)\right] \\
&\quad + \sum_{k=1}^{\infty} F_{t3_k}\sin\left[k\left(\theta_s + (n_3 - 1)\frac{2\pi S}{P}\right)\right] + \cdots + \sum_{k=1}^{\infty} F_{tP_k}\sin\left[k\left(\theta_s + (n_P - 1)\frac{2\pi S}{P}\right)\right] \Bigg\}
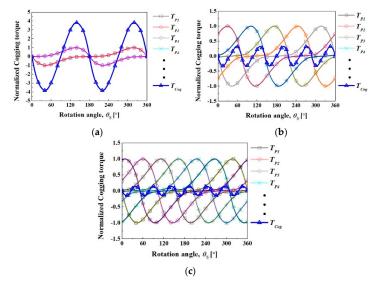\end{aligned} \tag{6}$$

where T_{pP} is the cogging torque that is generated by each pole, F_{tPk} is the 'k'th harmonic component of the tangential magnetic force density generated by each pole, $n_{2 \ldots P}$ are the order of the poles, P is the number of the poles, and S is the number of the slots. Here, the rotation angle of the rotor is expressed in the slot periodic angle.
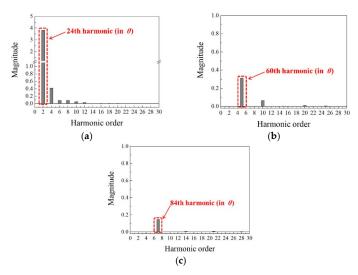
Figure 2. The geometry of the example model with multi poles and twelve teeth for (**a**) 8p/12s, (**b**) 10p/12s, and (**c**) 14p/12s.

Figure 3 shows the cogging torque of each example model case that resulted in the mutual interference of cogging torque for each pole. As can be seen from the figure, depending on the phase difference of each pole, the cogging torque can be increased or decreased by overlapping. Also, the harmonic component of cogging torque is demonstrated in Figure 4. Here, if those harmonic orders are calculated based on the mechanical angle (θ), the most dominant harmonic component has the order of least common multiple (LCM) of the number of slots and the number of poles. This is because the fundamental frequency of the cogging torque is calculated by using the LCM [26]. For example, since the LCM of an 8-pole/12-slot motor is 24, the 24th harmonic becomes as the most dominant harmonic component, as shown in Figure 4. This is a well-known fact of the cogging torque period and has been confirmed once again through this analysis.

Figure 3. Cogging torque caused by multi poles rotation based on θ_S: (**a**) cogging torque of 8p/12s, (**b**) cogging torque of 10p/12s, and (**c**) cogging torque of 14p/12s.

Figure 4. Harmonic spectra of cogging torque caused by multi poles rotation based on θ_s: (**a**) harmonics of 8p/12s, (**b**) harmonics of 10p/12s, and (**c**) harmonics of 14p/12s.

3. Mitigation Method of Slot Harmonic Cogging Torque Component

As the name implies, the slot harmonic component refers to a harmonic component that has the same number of cycles as the number of slots when the rotor rotates 360° (based on θ). Hence, in Equation (6), the first order harmonic component can be defined as the slot harmonic component (because of $\theta_s = 12\theta$). Then, the slot harmonic cogging torque can be expressed as follows:

$$
\begin{aligned}
T_{slot}(\theta_s) = RL_{stk}\Big\{ & F_{t1_1}\sin(\theta_s) + F_{t2_1}\sin\Big[\theta_s + (n_2-1)\tfrac{2\pi S}{P}\Big] \\
& + F_{t3_1}\sin\Big[\theta_s + (n_3-1)\tfrac{2\pi S}{P}\Big] + \cdots + F_{tP_1}\sin\Big[\theta_s + (n_P-1)\tfrac{2\pi S}{P}\Big]\Big\}
\end{aligned}
\tag{7}
$$

As can be seen from the result of Figure 4, when the motor is under the ideal condition and all the magnetic forces of each pole are equal to each other, the slot harmonic component does not exist in all cases. This is because the first harmonic component of each pole is canceled out by the phase difference from the other pole. This is easy to understand the phenomenon with the 8-pole/12-slot and 10-pole/12-slot models.

Substituting the number of poles of 8 and the number of slots of 12 into Equation (7), it is summarized as follows:

$$
\begin{aligned}
T_{slot}(\theta_s) &= RL_{stk}\Big\{ F_{t1_1}\sin(\theta_s) + F_{t2_1}\sin\Big[\theta_s + (2-1)\tfrac{2\pi\cdot12}{8}\Big] \\
&\quad + F_{t3_1}\sin\Big[\theta_s + (3-1)\tfrac{2\pi\cdot12}{8}\Big] + \cdots + F_{t8_1}\sin\Big[\theta_s + (8-1)\tfrac{2\pi\cdot12}{8}\Big]\Big\} \\
&= RL_{stk}\Big[\Big(F_{t1_1} + F_{t3_1} + F_{t5_1} + F_{t7_1}\Big)\sin(\theta_S) + \Big(F_{t2_1} + F_{t4_1} + F_{t6_1} + F_{t8_1}\Big)\sin(\theta_S + \pi)\Big].
\end{aligned}
\tag{8}
$$

As a result, in the motor of the 8-pole/12-slot, the cogging torque produced by each pole had two phases, and the phase difference was π. Therefore, under ideal conditions, the slot harmonic torque (first harmonic torque of each pole) becomes zero because each pole produces the same amount of magnetic force. Here, through the above equation, the removal condition of the slot harmonic can be more clearly expressed as follows:

$$
F_{t1_1} + F_{t3_1} + F_{t5_1} + F_{t7_1} = F_{t2_1} + F_{t4_1} + F_{t6_1} + F_{t8_1}
\tag{9}
$$

According to this condition, the slot harmonic component is likely to be canceled even if the density of each magnetic force does not exactly coincide. That is, even if the magnetic strength of each pole (the remanence of each magnet) is different, the slot harmonic component may be removed.

In this paper, since the influence of shape error and eccentricity is not considered, the above condition can be rearranged as follows using the relation of (2):

$$B_{r1}^2 + B_{r3}^2 + B_{r5}^2 + B_{r7}^2 = B_{r2}^2 + B_{r4}^2 + B_{r6}^2 + B_{r8}^2 \tag{10}$$

where $B_{r1\ ...\ rP}$ are the remanence of the magnet in each pole. Under this condition, the slot harmonic component can be mitigated, and all harmonics except the LCM harmonic component will be also mitigated by superposition because the phase difference is equal to the pole pitch.

As in the example of the 8-pole/12-slot motor, by substituting the number of poles of 10 and the number of slots of 12 into Equation (7), it can be summarized as follows:

$$
\begin{aligned}
T_{slot}(\theta_s) = \ & RL_{stk}\Big[\big(F_{t1_1} + F_{t6_1}\big)\sin(\theta_s) + \big(F_{t2_1} + F_{t7_1}\big)\sin\big(\theta_s + \tfrac{12}{5}\pi\big) \\
& + \big(F_{t3_1} + F_{t8_1}\big)\sin\big(\theta_s + \tfrac{24}{5}\pi\big) + \big(F_{t4_1} + F_{t9_1}\big)\sin\big(\theta_s + \tfrac{36}{5}\pi\big) \\
& + \big(F_{t5_1} + F_{t10_1}\big)\sin\big(\theta_s + \tfrac{48}{5}\pi\big)\Big].
\end{aligned}
\tag{11}
$$

Under ideal conditions, the slot harmonic torque (first harmonic torque of each pole) becomes zero because each pole produces the same amount of magnetic force. As a result, the removal condition of the slot harmonic can be expressed as follows:

$$F_{t1_1} + F_{t6_1} = F_{t2_1} + F_{t7_1} = F_{t3_1} + F_{t8_1} = F_{t4_1} + F_{t9_1} = F_{t5_1} + F_{t10_1} \tag{12}$$

$$B_{r1}^2 + B_{r6}^2 = B_{r2}^2 + B_{r7}^2 = B_{r3}^2 + B_{r8}^2 = B_{r4}^2 + B_{r9}^2 = B_{r5}^2 + B_{r10}^2. \tag{13}$$

Through the above examples, it is verified that the slot harmonic cogging torque can be zero, when the motor is under the ideal condition and all the magnetic forces of each pole are equal to each other regardless of the odd or even number of magnet set.

Looking at the process of deriving this condition, consequently, it is important to find poles with the same cogging torque phase so that the sum of the remanence of the magnets is equal to the poles with different phases. By using the equation below, the distance of pole (*N*), which has the same torque phase with the first (reference) pole, can be calculated in the pole number. This can be simply derived with the number of poles and the number of slots, and by taking into account the relationship between pole pitch and slot pitch.

$$N = \left| \frac{P}{(S-P)} \right| \tag{14}$$

According to Equation (14), *N* of the 14-pole/12-slot is assigned "7." Therefore, in the case of the 14-pole/12-slot, the torque phases of the first pole and the eighth pole are the same. Therefore, the slot harmonic torque removal condition for each pole/slot combination is derived as follows:

$$
\begin{aligned}
B_{r1}^2 + B_{r8}^2 &= B_{r2}^2 + B_{r9}^2 = B_{r3}^2 + B_{r10}^2 = B_{r4}^2 + B_{r11}^2 \\
&= B_{r5}^2 + B_{r12}^2 = B_{r6}^2 + B_{r13}^2 = B_{r7}^2 + B_{r14}^2.
\end{aligned}
\tag{15}
$$

In addition to the above condition, in order to make the magnetic flux connected to the winding uniform according to the polarity, the remanence summation of the entire magnets located at the N pole must be equal to that of the S pole. Therefore, the following condition should be also met:
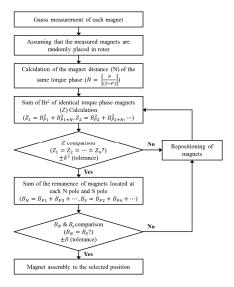
$$B_N(B_{r1} + B_{r3} + B_{r5} + \cdots) = B_S(B_{r2} + B_{r4} + B_{r6} + \cdots) \tag{16}$$

where B_N and B_S are total remanences of the north and south poles.

Considering these conditions when assembling magnets and rotors, the generation of the slot harmonic cogging torque components will be minimized. Hence, the work flow chart of the slot harmonic component mitigation method is shown in Figure 5. Here, the sum of $B_r{}^2$ of the poles with the same cogging torque phase is conveniently referred to as *Z*. The smaller the difference in *Z* value

for each torque phase is the smaller the slot harmonic size is. In addition, the tolerance is denoted as δ, and it is reasonable to choose this to be larger than the measurement uncertainty of the Gauss value of the magnet in practical.
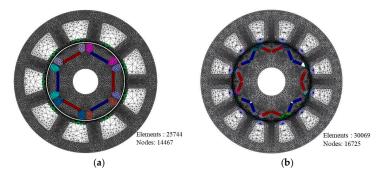

Figure 5. The workflow diagram of a method for mitigating slot harmonic cogging torque before rotor assembly.

4. Verification of the Proposed Method

4.1. Verification Using the Finite Element Analysis (FEA)

In this section, the FEA is conducted to verify the validity of the slot harmonic mitigation method proposed in Figure 5. Two example models are selected for this analysis. The first model is a 6-pole/9-slot interior permanent-magnet motor (IPM), and the other is an 8-pole/12-slot IPM. The geometry with the mesh information and the specification of each model are shown in Figure 6 and Table 1. Here, the saturation point of each core material was adjusted to be lower than the actual property. This is to confirm that the proposed method is still valid under nonlinear material properties.

In order to consider the unevenly magnetized magnet in FEA verification, firstly, the management tolerance on the B_r of the commercial magnets was investigated and is shown in Table 2. Then based on the data, the B_r of each magnet was randomly selected and positioned on the rotor, as shown in Figure 7. The selected B_r results and the magnet position are recorded in Tables 3 and 4. Here, in each table, Case A is each magnet arranged according to its number order, and Case B is where it is arranged according to the proposed method in Figure 5. The change in position of each magnet is shown more clearly in Figure 7. In Tables 3 and 4, it can be seen that the Z comparison and B_N-B_S comparison value are not 'zero,' even in Case B. In fact, since there is very low probability that there can be a magnet arrangement that satisfies this in reality, the tolerances were changed step by step to have the magnet array with the smallest comparison result.
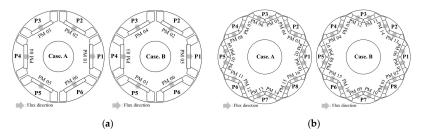
(**a**) (**b**)

Figure 6. The geometry and mesh information of each FEA model for the verification of the proposed method at (**a**) 6p/9s IPM and (**b**) 8p/12s IPM.

Table 1. Specification of each FEA model for the verification of the proposed method.

Item	6p/9s IPM	8p/12s IPM
Stator outer diameter	100.0 mm	150.0 mm
Rotor outer diameter	54.0 mm	82.0 mm
Stack length	40.0 mm	72 mm
Air gap length	1.0 mm	0.6 mm
Rated power	400 W	5000 W
Rated speed	3500 rpm	2000 rpm
Rated torque	1.1 Nm	23.8 Nm
Rated ph. current	10.3 Arms	120 Arms
Series turn per phase	72	20
Core material	50PN470 (FEM: saturate@1.2T)	50PN470 (FEM: saturate@1.2T)
Magnet material	NMX-36EH	NEOREC 40UH

Table 2. The magnet management tolerance of the manufacturer.

Company	6p/9s IPM	8p/12s IPM
TDK	NEOREC 40UH	1290 ± 30
	NEOREC 40TH	1285 ± 30
	NEOREC 38UX	1250 ± 30
	NEOREC 35NX	1200 ± 30
Hitachi	NMX-43SH	1295 ± 35
	NMX-41SH	1275 ± 35
	NMX-39EH	1235 ± 35
	NMX-36EH	1195 ± 35

(**a**) (**b**)

Figure 7. PM position change according to the proposed method for the FEA verification for (**a**) 6p/9s IPM and (**b**) 8p/12s IPM.

Table 3. Random selection of the magnet remanence for the 6p/9s model considering the management tolerance.

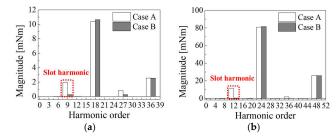| Position & Comparison	Case A		Case B	
	PM No.	B_r	PM No.	B_r
P1	PM 01	1.194 T	PM 05	1.226 T
P2	PM 02	1.195 T	PM 02	1.195 T
P3	PM 03	1.198 T	PM 04	1.162 T
P4	PM 04	1.162 T	PM 03	1.198 T
P5	PM 05	1.226 T	PM 01	1.194 T
P6	PM 06	1.172 T	PM 06	1.172 T
Z_1-Z_2	0.212 (T)2		0.042 (T)2	
B_N-B_S	0.089 (T)		0.017 (T)	

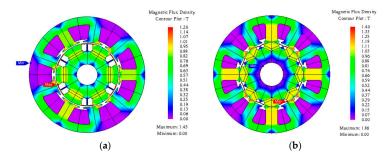**Table 4.** Random selection of the magnet remanence of 8p/12s model considering the management tolerance.

Position & Comparison	Case A		Case B	
	PM No.	B_r	PM No.	B_r
P1	PM 01	1.265 T	PM 05	1.269 T
	PM 02	1.275 T	PM 06	1.278 T
P2	PM 03	1.290 T	PM 13	1.287 T
	PM 04	1.291 T	PM 14	1.285 T
P3	PM 05	1.269 T	PM 11	1.309 T
	PM 06	1.278 T	PM 12	1.309 T
P4	PM 07	1.294 T	PM 03	1.290 T
	PM 08	1.295 T	PM 04	1.291 T
P5	PM 09	1.278 T	PM 07	1.294 T
	PM 10	1.290 T	PM 08	1.295 T
P6	PM 11	1.309 T	PM 15	1.310 T
	PM 12	1.309 T	PM 16	1.315 T
P7	PM 13	1.287 T	PM 09	1.278 T
	PM 14	1.285 T	PM 10	1.290 T
P8	PM 15	1.310 T	PM 01	1.265 T
	PM 16	1.315 T	PM 02	1.275 T
Z_1-Z_2	−0.483 (T)2		0.009 (T)2	
B_N-B_S	−0.187 (T)		0.004 (T)	

Now, the validity of the proposed method can be verified by examining the variation of the cogging torque harmonic component in each case. The FEA results of the cogging torque harmonic component are shown in Figure 8. Figure 8a shows the result of the 6-pole/9-slot model, and Figure 8b shows the result of the 8-pole/12-slot model. In both models, it can be seen that the slot harmonic component of Case B is much smaller than Case A. Therefore, the proposed method was effective in mitigating the slot harmonic component of cogging torque. Furthermore, it can be seen that the permeability of the core is in a somewhat non-linear region by observing the flux density distribution in Figure 9. Hence, although we ignored the saturation when deriving the method, the result of Figure 8 proves that the proposed method is still effective under the non-linear material characteristics of the ferromagnetic.

Figure 8. FEA results of cogging torque harmonic component according to each case: (**a**) 6p/9s IPM and (**b**) 8p/12s IPM.

Figure 9. Contour plot of magnetic flux density under no load condition for (**a**) 6p/9s IPM and (**b**) 8p/12s IPM.

4.2. Verification with Experimentation

For the experimental verification, both models in Figure 6 were manufactured, one of each. Figure 10 is a picture of the produced motor. Then, the experiment process was performed as follows.
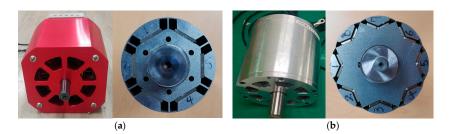

Figure 10. The manufactured motors for the experiment: (**a**) 6p/9s IPM and (**b**) 8p/12s IPM.

1. The surface Gauss value of each magnet was measured (with ATM 1000, SCMI) in the space, excluding the magnetic substance. Figure 11 shows a picture of the measurement, and the results are written in Tables 5 and 6. The Gauss average value was calculated from the seven measurement points per each magnet, and the measurement uncertainty was calculated by repeating the measurement five times.

2. The position of each magnet was set according to the proposed method. The results are shown in Tables 5 and 6 and in Figure 12 (Case B).

3. These magnets were alternately assembled to the rotor according to the case of each model shown in Figure 12, and the cogging torque according to each case was measured (with ATM-5KA, SUGAWARA) as shown in Figure 13.
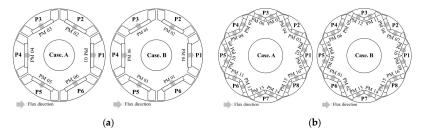
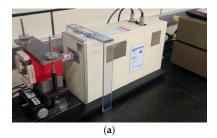**Figure 11.** Gauss measurement of the magnet surface.

Table 5. Gauss measurement of each magnet surface of the 6p/9s model and the changes in magnet position according to the proposed method.

Position & Comparison	Case A		Case B	
	PM No.	Gauss Avg.	PM No.	Gauss Avg.
P1	PM 01	194.3 mT	PM 04	198.4 mT
P2	PM 02	198.3 mT	PM 02	198.3 mT
P3	PM 03	196.7 mT	PM 05	196.9 mT
P4	PM 04	198.4 mT	PM 06	199.1 mT
P5	PM 05	196.9 mT	PM 03	196.7 mT
P6	PM 06	199.1 mT	PM 01	194.3 mT
Uncertainty	±0.2%			
Z_1-Z_2	−3113.3 (mT)2		106.9 (mT)2	
B_N-B_S	−7.9 (mT)		0.3 (mT)	

The results of cogging torque measurements are demonstrated in Figure 14. Figure 14a shows the result of the 6-pole/9-slot motor. Case A had a cogging torque of 56.7 mNm$_{pk-pk}$, and Case B had 55.1 mNm$_{pk-pk}$. In Figure 14b the 8-pole/12-slot motor showed 227.3 mNm$_{pk-pk}$ for Case A and 214.8 mNm$_{pk-pk}$ for Case B. As a result, although the shapes of the stator and rotor of the analyzed motors were already optimized for reducing cogging torque, the cogging torque could be improved more by using the proposed method. The main cause of this cogging difference between Case A and B is due to the slot harmonic component of Case B being smaller than Case A, as can be seen in the FFT result of each cogging torque in Figure 15. Consequently, the validity of the proposed method was confirmed again by the experimental results. Overall, since this method only affects the position of each magnet before assembly, it can be compatible with the conventional cogging torque reduction methods using the teeth curvature and rotor shape modulation.

(a)   (b)

Figure 12. PM position change according to the proposed method for the experimental verification for (**a**) 6p/9s IPM and (**b**) 8p/12s IPM.
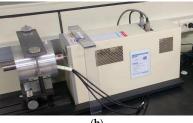
(**a**)　　　　　　　　　　　　　　(**b**)

Figure 13. Cogging torque measurement of each motor for (**a**) 6p/9s IPM and (**b**) 8p/12s IPM.

Table 6. Gauss measurement of each magnet surface of the 8p/12s model and the changes in magnet position according to the proposed method.

Position & Comparison	Case A		Case B	
	PM No.	Gauss Avg.	PM No.	Gauss Avg.
P1	PM 01	227.1 mT	PM 09	225.5 mT
	PM 02	228.7 mT	PM 10	226.2 mT
P2	PM 03	233.8 mT	PM 07	231.1 mT
	PM 04	234.0 mT	PM 08	231.5 mT
P3	PM 05	226.3 mT	PM 11	230.6 mT
	PM 06	226.8 mT	PM 12	230.9 mT
P4	PM 07	231.2 mT	PM 05	226.3 mT
	PM 08	231.5 mT	PM 06	226.8 mT
P5	PM 09	225.5 mT	PM 03	233.9 mT
	PM 10	226.2 mT	PM 04	234.0 mT
P6	PM 11	230.6 mT	PM 01	227.1 mT
	PM 12	230.9 mT	PM 02	228.7 mT
P7	PM 13	229.0 mT	PM 13	229.0 mT
	PM 14	229.9 mT	PM 14	229.9 mT
P8	PM 15	234.2 mT	PM 15	234.2 mT
	PM 16	234.3 mT	PM 16	234.2 mT
Uncertainty	±0.1%			
Z_1-Z_2	−10,065.1 (mT)2		133.9 (mT)2	
B_N-B_S	−21.9 (mT)		0.3 (mT)	

(**a**)　　　　　　　　　　　　　　(**b**)

Figure 14. The measured cogging torque of each motor for (**a**) 6p/9s IPM and (**b**) 8p/12s IPM.
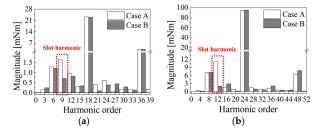

(**a**)　　　　　　　　　　　　　　(**b**)

Figure 15. Cogging torque measurement of each motor for (**a**) 6p/9s IPM and (**b**) 8p/12s IPM.

5. Discussion

The reduction effect cannot be clearly seen in the peak-peak comparison of cogging torque in Figure 14. This is because the LCM component is much larger than the slot harmonic component in both cases. In this case, although the slot harmonic component was reduced, as shown in Figure 15, by the proposed method, the effect is not seen much. If the proposed method is applied to a model that is sensitive to the slot harmonic component, the cogging torque can be effectively mitigated, compared with the results of this paper. In other words, the proposed method has a different effect on the mitigation of cogging torque depending on which harmonic component is dominant.

Additionally, since there are some methods to measure the B_r or flux density of PM, the real application for applying the proposed method can be manufactured. Among the measurement methods, the simplest example is using Helmholtz coil. As mentioned in the introduction, the proposed method is more appropriate for small quantity customized production than mass production because the Gauss value of each magnet should be measured before the assembly. In the case of mass production, it is possible that if the manufacturing tolerance of the magnetization yoke is adjusted based on the principle of the slot harmonic component mitigation condition, that the influence of the uneven magnetization can be alleviated.

As described above, there are some limitations to the proposed method. However, it is meaningful that we have dealt with the method to compensate manufacturing tolerance (Uneven PM) that has not been covered in the meantime. Furthermore, this method can prevent an increase in cogging torque caused by unevenly magnetized PMs of motors with a high number of poles. Since small scale customized manufacturing process, which adopts the method of the pre-magnetization of magnets before assembly, cannot adjust and compensate for the unevenness of the PMs, by using the proposed method, it will be possible to ensure the cogging performance of a manufactured motor.

6. Conclusions

In this study, a mitigation method of slot harmonic cogging torque caused by the unevenly magnetized magnet was proposed. This method was drawn through the qualitative analysis of the cogging torque from a macroscopic perspective. As shown in Figure 5, the main process of this method is arranging each magnet according to the non-slot harmonic condition described in Section 3. The validity of the proposed method was verified using FEA and experimentation. Here, the verification was performed by comparing the harmonic components of the cogging torque with and without the proposed method. In this process, it was confirmed that this method is sufficiently effective, even when considering the non-linear material characteristics of the ferromagnetic.

References

1. Li, G.J.; Ren, B.; Zhu, Z.Q.; Li, Y.X.; Ma, J. Cogging torque mitigation of modular permanent magnet machines. *IEEE Trans. Magn.* **2016**, *52*, 1–10. [CrossRef]
2. Park, Y.U.; Cho, J.H.; Kim, D.K. Cogging torque reduction of single-phase brushless DC motor with a tapered air-gap using optimizing notch size and position. *IEEE Trans. Ind. Appl.* **2015**, *51*, 4455–4463. [CrossRef]

3. Xue, Z.; Li, H.; Zhou, Y.; Ren, N.; Wen, W. Analytical prediction and optimization of cogging torque in surface-mounted permanent magnet machines with modified particle swarm optimization. *IEEE Trans. Ind. Electron.* **2017**, *64*, 9795–9805. [CrossRef]

4. Ren, W.; Xu, Q.; Li, Q.; Zhou, L. Reduction of cogging torque and torque ripple in interior PM Machines with asymmetrical V-type rotor design. *IEEE Trans. Magn.* **2016**, *52*, 1–5. [CrossRef]

5. Dosiek, L.; Pillay, P. Cogging torque reduction in permanent magnet machines. *IEEE Trans. Ind. Appl.* **2007**, *43*, 1565–1571. [CrossRef]

6. Kim, K. A novel method for minimization of cogging torque and torque ripple for interior permanent magnet synchronous motor. *IEEE Trans. Magn.* **2014**, *50*, 793–796. [CrossRef]

7. Wang, D.; Wang, X.; Jung, S. Cogging torque minimization and torque ripple suppression in surface-mounted permanent magnet synchronous machines using different magnet widths. *IEEE Trans. Magn.* **2013**, *49*, 2295–2298. [CrossRef]

8. Wanjiku, J.; Khan, M.A.; Barendse, P.S.; Pilay, P. Influence of slot openings and tooth profile on cogging torque in axial-flux pm machines. *IEEE Trans. Ind. Electron.* **2015**, *62*, 7578–7589. [CrossRef]

9. Kwon, J.; Lee, J.; Zhao, W.; Kwon, B. Flux-switching permanent magnet machine with phase-group concentrated-coil windings and cogging torque reduction technique. *Energies* **2018**, *11*, 2758. [CrossRef]

10. Hwang, M.; Lee, H.; Cha, H. Analysis of torque ripple and cogging torque reduction in electric vehicle traction platform applying rotor notched design. *Energies* **2018**, *11*, 3053. [CrossRef]

11. Dini, P.; Saponara, S. Cogging torque reduction in brushless motors by a nonlinear control technique. *Energies* **2019**, *12*, 2224. [CrossRef]

12. Kim, J.M.; Yoon, M.H.; Hong, J.P.; Kim, S.I. Analysis of cogging torque caused by manufacturing tolerances of surface-mounted permanent magnet synchronous motor for electric power steering. *IEEE Trans. Electr. Power Appl.* **2016**, *10*, 691–696. [CrossRef]

13. Ortega, A.J.P.; Paul, S.; Islam, R.; Xu, L. Analytical model for predicting effects of manufacturing variations on cogging torque in surface-mounted permanent magnet motors. *IEEE Trans. Magn.* **2016**, *52*, 3050–3061. [CrossRef]

14. Qian, H.; Guo, H.; Wu, Z.; Ding, X. Analytical solution for cogging torque in surface-mounted permanent-magnet motors with magnet imperfections and rotor eccentricity. *IEEE Trans. Magn.* **2014**, *50*, 1–15. [CrossRef]

15. Zhou, Y.; Li, H.; Meng, G.; Zhou, S.; Cao, Q. Analytical calculation of magnetic field and cogging torque in surface-mounted permanent-magnet machines accounting for any eccentric rotor shape. *IEEE Trans. Ind. Electron.* **2015**, *62*, 3438–3447. [CrossRef]

16. Lee, C.J.; Jang, G.H. Development of a new magnetizing fixture for the permanent magnet brushless dc motors to reduce the cogging torque. *IEEE Trans. Magn.* **2011**, *47*, 2410–2413. [CrossRef]

17. Song, J.Y.; Kang, K.J.; Kang, C.H.; Jang, G.H. Cogging torque and unbalanced magnetic pull due to simultaneous existence of dynamic and static eccentricities and uneven magnetization in permanent magnet motors. *IEEE Trans. Magn.* **2014**, *50*, 1–9. [CrossRef]

18. Sung, S.J.; Park, S.J.; Jang, G.H. Cogging torque of brushless DC motors due to the interaction between the uneven magnetization of a permanent magnet and teeth curvature. *IEEE Trans. Magn.* **2011**, *47*, 1923–1928. [CrossRef]

19. Ou, J.; Liu, Y.; Qu, R.; Doppelbauer, M. Experimental and theoretical research on cogging torque of PM synchronous motors considering manufacturing tolerances. *IEEE Trans. Ind. Electron.* **2018**, *65*, 3772–3783. [CrossRef]

20. Ionel, D.M.; Popescu, M.; McGilp, M.I.; Miller, T.J.E.; Dellinger, S.J. Assessment of torque components in brushless permanent-magnet machines through numerical analysis of the electromagnetic field. *IEEE Trans. Electr. Power Appl.* **2005**, *41*, 1149–1158. [CrossRef]

21. Zhu, W.; Pekarek, S.; Fahimi, B.; Deken, B.J. Investigation of force generation in a permanent magnet synchronous machine. *IEEE Trans. Energy Convers.* **2007**, *22*, 557–565. [CrossRef]

22. Meessen, K.J.; Paulides, J.J.H.; Lomonova, E.A. Force calculations in 3-D cylindrical structures using fourier analysis and the Maxwell stress tensor. *IEEE Trans. Magn.* **2013**, *49*, 536–545. [CrossRef]

23. Gao, J.; Wang, G.; Liu, X.; Zhang, W.; Huang, S.; Li, H. Cogging torque reduction by elementary-cogging-unit shift for permanent magnet machines. *IEEE Trans. Magn.* **2017**, *53*, 1–5. [CrossRef]

24. Zhu, Z.Q.; Ruangsinchaiwanich, S.; Howe, D. Synthesis of cogging-torque waveform from analysis of a single stator slot. *IEEE Trans. Ind. Appl.* **2006**, *42*, 650–657. [CrossRef]

25. Zhu, Z.Q.; Ruangsinchaiwanich, S.; Chen, Y.; Howe, D. Evaluation of superposition technique for calculating cogging torque in permanent-magnet brushless machines. *IEEE Trans. Magn.* **2006**, *42*, 1597–1603. [CrossRef]

26. Gieras, J.F. *Electrical Machines: Fundamentals of Electromechanical Energy Conversion*; CRC Press: Boca Raton, FL, USA, 2016.